Potential of remote sensing and open street data for flood mapping in poorly gauged areas: a case study in Gonaives, Haiti

A. Bozza, A. Durand, G. Confortola, A. Soncini, B. Allenbach & D. Bocchiola

Applied Geomatics

ISSN 1866-9298

Appl Geomat
DOI 10.1007/s12518-016-0171-x

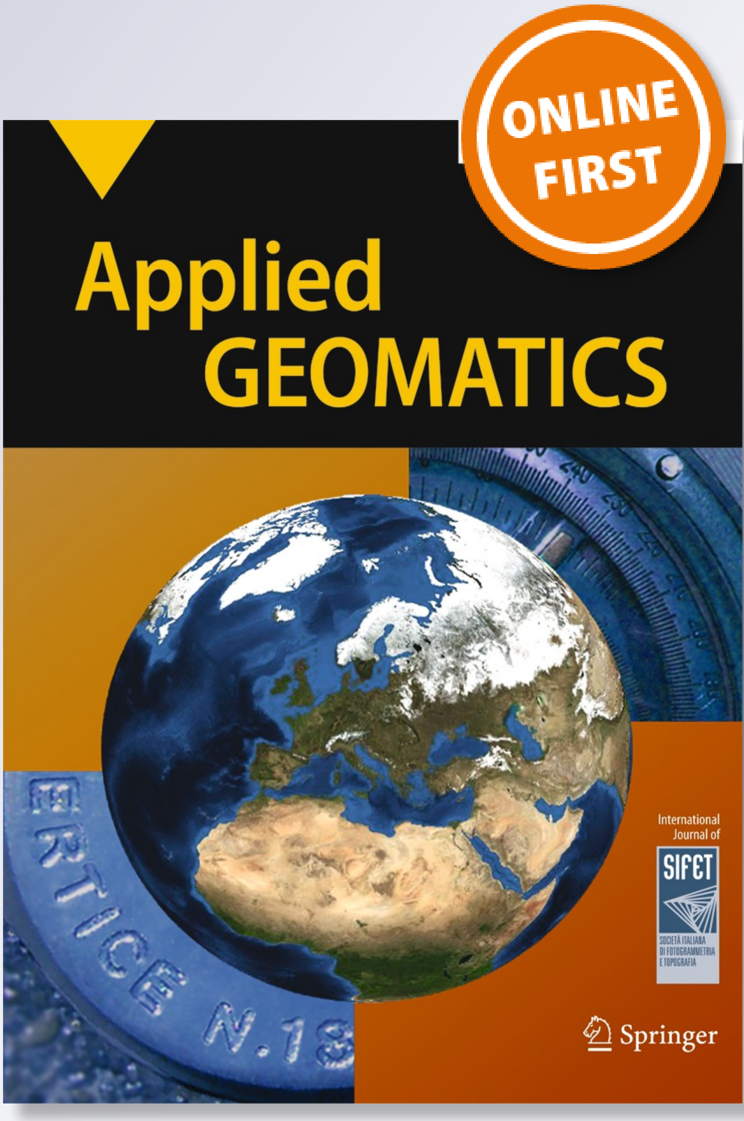

Springer

Appl Geomat
DOI 10.1007/s12518-016-0171-x

ORIGINAL PAPER

Potential of remote sensing and open street data for flood mapping in poorly gauged areas: a case study in Gonaives, Haiti

A. Bozza [1,2] · A. Durand [2] · G. Confortola [1] · A. Soncini [1] · B. Allenbach [2] · D. Bocchiola [1,3]

Received: 15 January 2016 / Accepted: 17 February 2016

Abstract The Hispaniola Island, in the Caribbean tropical zone, is prone to extreme flood events. Floods are caused by tropical springs and hurricanes and may lead to human losses, economical damages, and spreading of waterborne diseases. Flood studies based upon hydrological and hydraulic modelling are hampered by almost complete lack of hydrometeorological data. Thenceforth, and given the cost and complexity in the organization of field measurement campaigns, the need for exploitation of remote sensing data, and open source data bases. We present here a feasibility study to explore the potential of (i) high-resolution of digital elevation models (DEMs) from remote imagery and (ii) remotely sensed precipitation data, to feed hydrological flow routing and hydraulic flood modelling, applied to the case study of river La Quinte closed to Gonaives (585 km^2), Haiti. We studied one recent flood episode, namely hurricane Ike in 2008, when flood maps from remote sensing were available for validation. The atmospheric input given by hourly rainfall was taken from downscaled Tropical Rainfall Measuring Mission (TRMM) daily estimates, and subsequently fed to a semi-distributed DEM-based hydrological model, providing an hourly flood hydrograph. Then, flood modelling using Hydrologic Engineering Center River Analysis System (HEC-RAS 1D, one-dimensional model for unsteady open channel flow) was carried out under different scenarios of available digital elevation models. The DEMs were generated using optical remote sensing satellite WorldView-1 and Shuttle Radar Topography Mission (SRTM), combined with information from an open source database (OpenStreetMap). Observed flood extent and land use have been extracted using *Système Pour l'Observation de la Terre*-4 (SPOT-4) imagery. The hydraulic model was tuned for floodplain friction against the observed flooded area. We compared different scenarios of flood simulation and the predictive power given by model tuning. Our study provides acceptable results in depicting flooded areas, especially considering the tremendous lack of ground data, and shows the potential of hydrological modelling approach fed by remote sensing information in Haiti, and in similarly data-scarce areas. Our approach may be useful to provide depiction of flooded areas for the purpose of (i) flood design for urban planning under a frequency-driven approach and (ii) forecasting of flooded areas for warning procedures, pending availability of weather forecast with proper lead time.

Keywords Flood mapping · Hydraulic modelling · Remote sensing · Digital elevation models · Haiti

Electronic supplementary material The online version of this article (doi:10.1007/s12518-016-0171-x) contains supplementary material, which is available to authorized users.

✉ D. Bocchiola
daniele.bocchiola@polimi.it

[1] Hydrology Division, Department of ICA, Politecnico di Milano, 32 Leonardo da Vinci Sq, 20133 Milano, Italy

[2] SERTIT, University of Strasbourg, Pole API - Parc d'innovation, 300 Boulevard Sébastien Brant, BP 10413, 67412 Illkirch Graffenstaden, France

[3] EVK2CNR Association, San Bernardino 145, 24126 Bergamo, Italy

Introduction

The Island of Hispaniola, in the Caribbean tropical zone, is prone to extreme flood events. Particularly, Haiti's basins are increasingly affected by tropical springs and hurricanes, which may carry large death toll, economic damages, and medical emergencies, including cholera epidemics (Rinaldo et al., 2012), as occurred in the wake of

Published online: 26 February 2016

the earthquake on January 12, 2010 (magnitude 7.0). It is therefore necessary to build a flood modelling approach for aiding (i) land use planning, (ii) setup of flood proofing strategies, (iii) real-time flood forecasting and warning procedures, and (iv) priority-driven emergency measures for first aid and waterborne disease containment. Flood mapping towards these ends is hampered by two main flaws, namely (i) lack of fine topographic information and (ii) lack of hydro-meteorological data. This is a typical ground for exploitation of the potential given by remote sensing technologies and GISs. Remote sensing data can reduce the effect of uncertainty on predictions (e.g. Bates, 2004; Hunter et al., 2005; Horritt, 2006; Horritt et al., 2007; Di Baldassarre, 2009; Mason et al., 2009; Schumann et al., 2009; Stephens et al., 2012), and use of remotely sensed maps of flood extent (Smith et al., 1997; Bates et al., 1997; Horritt et al., 2001) also for flood models validation (Horritt, 2000) is widespread nowadays. When it comes to numerical flood modelling, a key issue is the complexity of flow within floodplains, and especially the depiction of small-scale topographic features and hydrodynamic control exerted therein (Yamazaki et al., 2012). Hydrodynamic modelling requires a combination of detailed topographic features, such as small channels, rivers, roads and squares, walls, etc. to realistically represent the complexity of the flow system within urban areas. Recent advances in remote sensing technologies widened the range of available topographic data, and now various kinds of digital elevation models (DEMs) are accessible (Yamazaki et al., 2012). Nowadays, scientists and practitioners have access to spatially detailed and accurate data and information, appropriate for validating the performance of distributed models, at scales suitable to describe the underlying process variability (Bates, 2012). An important breakthrough came with the advent of remote sensing techniques for wide-area topographic mapping, most notably airborne laser altimetry (Gomes-Pereira and Wicherson, 1999; Marks and Bates, 2000; French, 2003; Bates et al., 2003). Contrarily to expensive airborne DEMs, such as Light Detection and Ranging (LiDAR) characterized by vertical accuracy of few centimetres but limited spatial coverage, spaceborne DEMs, like Shuttle Radar Topography Mission (SRTM) and Advanced Spaceborne Thermal Emission and Reflection Radiometer (ASTER) Global Digital Elevation Model, are freely available and cover large portions of the globe.

We present here a feasibility study to explore potential of (i) high-resolution imagery combined with information from open source data and (ii) weather information from remote sensing, to aid (iii) prediction of flooding in the case study area of Gonaives, Haiti. We focus on the case study event of hurricane Ike in 2008, when retrieval of the necessary data to set up our procedure was possible.

Meteorological data, i.e. rainfall estimates from Tropical Rainfall Measuring Mission (TRMM) satellite, have been used to gather precipitation amount and subsequently fed to a minimal hydrological model (Bocchiola et al., 2011) for flow routing, necessary for flood hydrograph assessment. The flood hydrograph so obtained was then fed to Hydrologic Engineering Center River Analysis System (HEC-RAS 1D, one dimensional model for unsteady open channel flow) for flood mapping. HEC-RAS 1D modelling has been applied under different scenarios, characterized by a combination of original "crude" DEMs and topographic information obtained from local, open source databases. Through a benchmarking of the model's results in representing flooded areas against *Système Pour l'Observation de la Terre*-4 (SPOT-4, a French satellite) flood images, we tested the effect of refining DEMs resolution in providing accurate description of flooding extent.

Case study

Target area

The study area is River La Quinte basin closed to Gonaives, Haiti (Fig. 1). The catchment domain is 585 km^2, and the area of interest, where we carry out the validation of DEMs is a 15-km^2 reach (covered by WorldView-1) around the urban area of Gonaives. This area was chosen because hurricane Ike impact was monitored therein via satellite imagery and because it was the only part of Gonaives where we had available world-view images (red polygon in Fig. 1) used to generate the DEM. A SPOT-4 image, acquired within the framework of the International Charter Space and Major Disaster, depicting post event (September 9, 2008) flooded areas, was used for flood model validation. The digital elevation model used for hydraulic simulation came from the Shuttle Radar Topography Mission (SRTM) and from WorldView-1 satellite imageries. DigitalGlobe WorldView-1 stereo-pair satellite produces panchromatic, half-meter resolution imagery, and it is efficient at in-track stereo collection (for an overview of WorldView-1 features, see e.g. Satimagingcorp, 2012). The stereo capability of WorldView-1 sensor provides the opportunity to extract high-resolution digital elevation models. The extracted DEM has a vertical root mean square (RMS) accuracy within 1.5 m when using accurate ground control points (GCPs) and approximately within 5 m RMS accuracy when using no GCPs. The elevation model was created in a standard stereoscopic configuration with LPS (Erdas Imagine software), but unfortunately, it was extracted using two images acquired at different dates (22 January 2010 and 28 November 2009). The RMS of positioning accuracy is low within the urban area (5 m), and the pixel size is of 1 m. SRTM is a 3-arc-seconds DEM created during the NASA's SRTM (2012) with a vertical noise approximately 6 m at 90-m spatial resolution (using GCPs). This product has successfully been used in flood

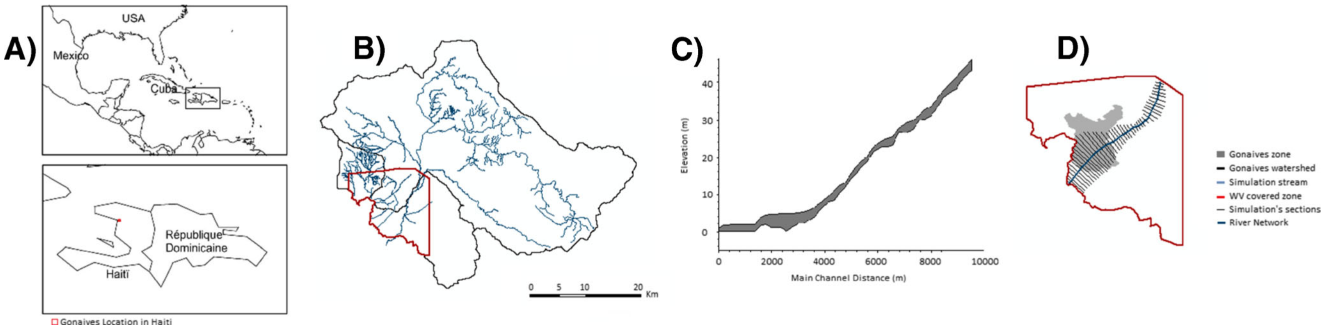

Fig. 1 **a** Position of Haiti and Gonaives location; **b** River La Quinte basins, Gonaives watershed and WorldView-1-covered zone; **c** longitudinal profile for HEC-RAS simulation; **d** Cross-sections for HEC-RAS simulation

models (Sanders, 2007). The detailed topographic features used to ameliorate DEM products came here from OpenStreetMap (http://www.openstreetmap.org/). The latter is a free, open source map created by volunteers all over the globe. It was used here to localize roads and canal networks for improved depiction of flood dynamics. Land use classification was extracted from a SPOT-5 image acquired on September 7, 2007. Land use was also used to select Manning's (i.e. hydraulic roughness) coefficients within HEC-RAS environment that were subsequently analysed for sensitivity and to keep into account buildings within SRTM.

Hurricane Ike event

On September 6, 2008, the town of Gonaives suffered the passage of hurricane Ike. The roads were flooded and hundreds of houses destroyed. Hurricane Ike reached force 4 and was the last of a series of four hurricanes at 5–7 days interval (Gustave, Fay, and Hanna). On September 1, Hanna, the strongest hurricane which hit the north-west coast of Haiti, caused 529 victims therein, 495 only in Gonaives, and 300, 000 persons have been affected. This heavy toll adds to the 50 victims of tropical storm Fay (on August 15–16) and 75 others of hurricane Gustav (August 26). The extremely high number of victims in the city of Gonaives is due to heavy floods that hit the city during the passage of the storms. The torrential rains that lashed the city raised the water level in the streets up to 5 m (France24, 2013; NOAA, 2012). During the same week of hurricanes Hanna and Ike, TRMM satellite estimated the highest daily rainfall in Gonaives watershed into 216 mm. According to our calculation, an estimated (average) daily peak flow of 315 $m^3 s^{-1}$ may have resulted therein. The SPOT-4 satellite image has been acquired upon September 9 2008, and used to infer flooded surface for model validation. The satellite carries a HRVIR optical sensor able to deliver visible and infrared bands at 20-m resolution. A raster map of the high and low flooded level set has been produced by Sérvice Régional de Traitement d'Image et de Teledétection (SERTIT-University of Strasbourg) within the framework of the International Charter Space and Major Disaster. The layers have been produced by a pixel-oriented spectral analysis using the near-infrared and mid-infrared bands of the SPOT sensor (Yesou et al., 2003). High-level flooded state is extracted by detecting persistent, visible water on the image. Low-level flooded state is extracted by detecting high water marks, mud, and humidity traces. The low flooded class has been later ignored during the validation of our results, to compare only persistently flooded sites (Fig. 2).

Methods

DEMs refinement

In Fig. 3, a flow chart of data and steps of our methodology of the study is proposed. The procedure set out is a semi-automatic one, carried out with different softwares, including Matlab, Erdas Imagine, ArcGis, HEC-GeoRAS. The first step is DEM refinements. The purpose of this procedure is to enhance small-scale topographic features, because a first-order control on flooding dynamics is imposed by topography and the accuracy of flooding maps may be reduced by coarse resolution of the imagery. WorldView-1- and SRTM-based DEMs seem not sufficiently detailed to provide a fine description of floodplain connectivity within an intricate urban environment as here. To test such hypothesis and yield potential improvement of urban floods representation, these DEMs have been used as HEC-RAS model background, either in their raw format or with topographic refinement (Fig. 4).

Gonaives urban area features increasing paving of roads, weak levees of in town streams, and a poor drainage system (often clogged by waste). Consequently, after intense precipitation episodes, roads act mostly like channels, only bounded by buildings. Thenceforth, the network of buildings and roads need to be accurately depicted to provide a likely representation of water fluxes in town. Our original topographic information (from DEMs) has been filled with OpenStreetMap database, used as a reference for drainage network and urban geometry structure. Geospatial information (roads and waterways network) selected by OpenStreetMap has been used

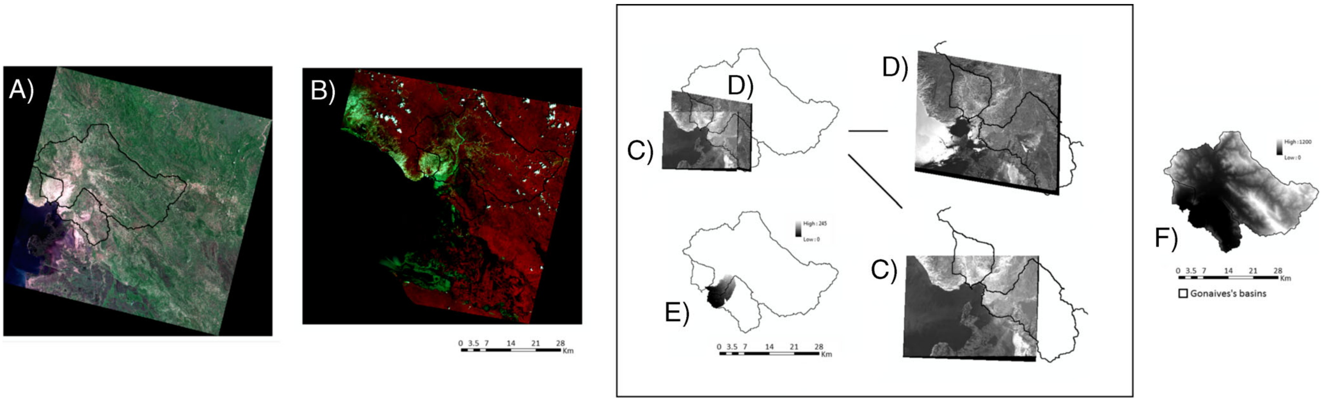

Fig. 2 Remote sensing images employed during the study: SPOT-5 (**a**), SPOT-4 (**b**), WorldView-1 22/01/2010 (**c**), WorldView-1 28/11/2009 (**d**), WorldView-1-extracted DEM (**e**), and SRTM (**f**)

in the form of buffered polygons with different width sections according to their own characteristics. The WorldView-1-based DEM was modified by artificially imposing canals and roads, i.e. by inserting proper hollow areas within the DEM. Then, the DEM was smoothed using a 3 × 3 moving average window (from Focal Statistics in Spatial Analyst toolbox available in ArcGIS 10), and the function “Fill” (from the Spatial Analyst

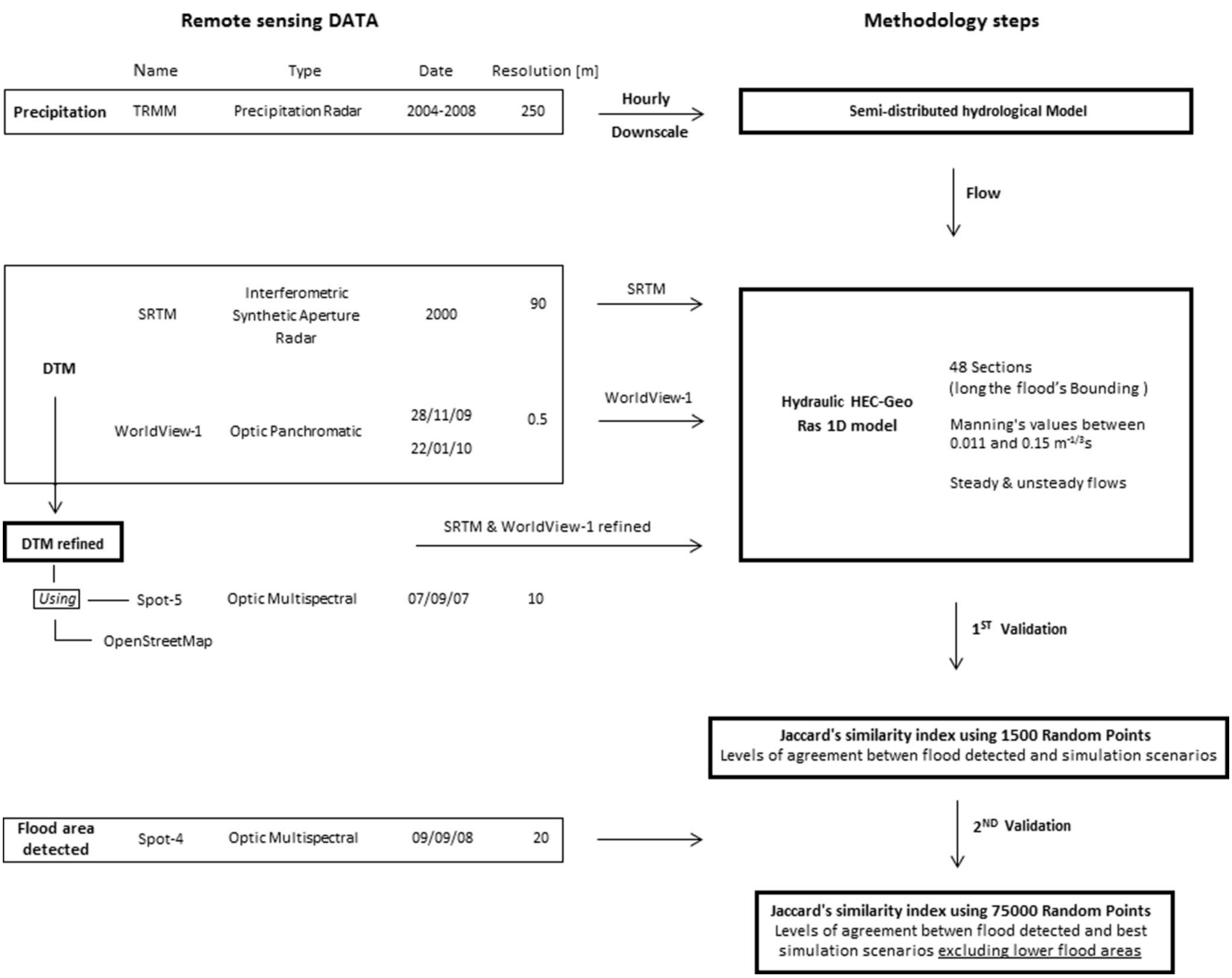

Fig. 3 Flow chart of used data and methods for the study

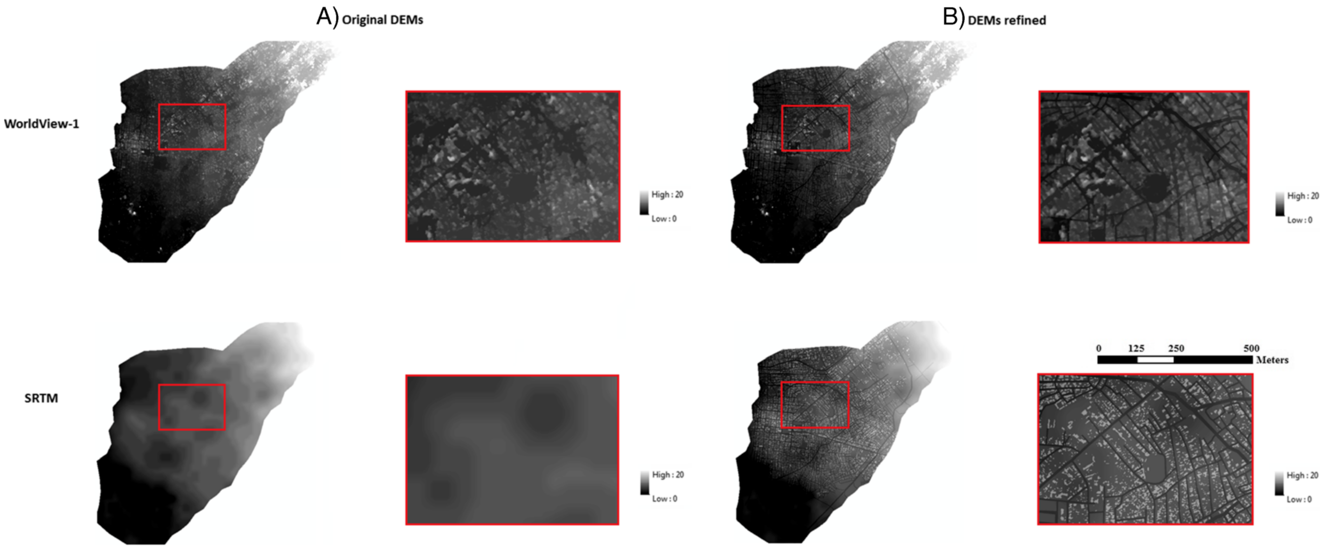

Fig. 4 Original DEMs (**a**) and refined DEMs (**b**) extracted into the simulation areas, zoomed (*red squares*) in Gonaives central area. The same color scale was used for all DEMs

toolbox available in ArcGIS 10) was used to fill the sinks so obtained.

The same procedure was applied upon the SRTM, which was resampled and smoothed at 1-m resolution. Due to SRTM low spatial resolution, it was not possible to visualize buildings therein.

While building extent could be identified using SPOT-5 above, their actual height could not. So, we decided here to provide a fixed altitude and examined three different scenarios, namely 3, 5, and 7 m, to investigate potential overtopping and possible (noticeable) changes in flooded areas. However, the results were little sensitive to this choice, given that flow depth rarely exceeded 2 m or so, and we chose to use 5 m, which is largely enough to avoid overtopping of buildings by flood. Figure 5 shows the information added to our database, displaying that detection of a building and use of OpenStreetMap information to modify DEM may provide refined representation of the urban network. Observing the bed elevation profile (used in HEC-RAS model) of the four different DEM scenarios so built (Fig. 6), one notices how the altimetry of the same cross-sections evolves in each DEM's representation.

Precipitation input and semi-distributed hydrological model

Daily rainfall as estimated from TRMM satellite was used to provide the precipitation input for hydrological flow routing simulation. Here, TRMM provides the only available source of information about precipitation in Haiti that we know of, given that observations from ground networks were not

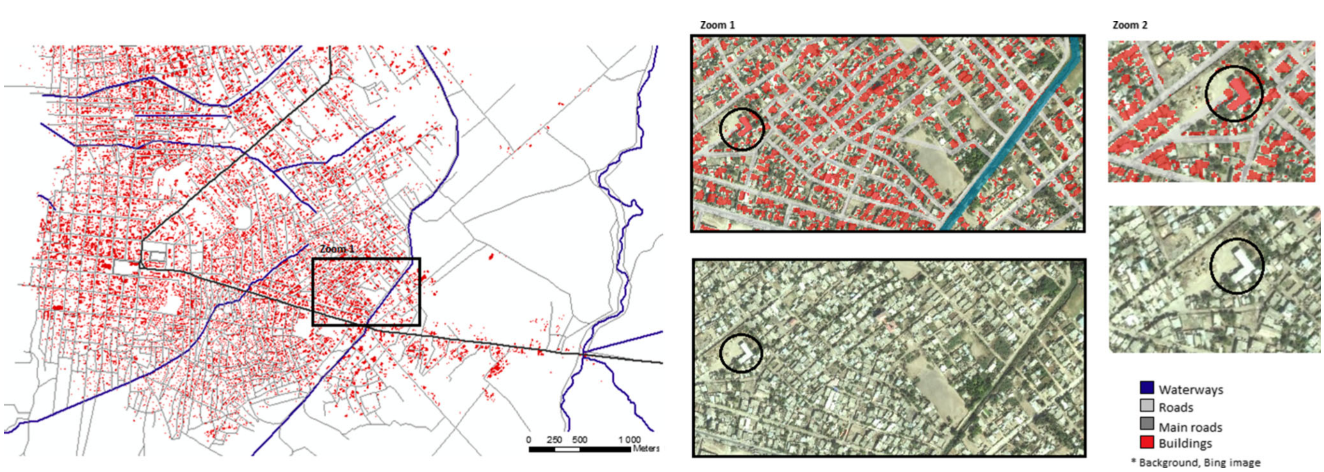

Fig. 5 Geospatial information derived from OpenStreetMap (roads and waterways network) and buildings geometry extracted from SPOT-5. The zoom of Gonaives central area highlights the accuracy of network buffering and buildings extraction

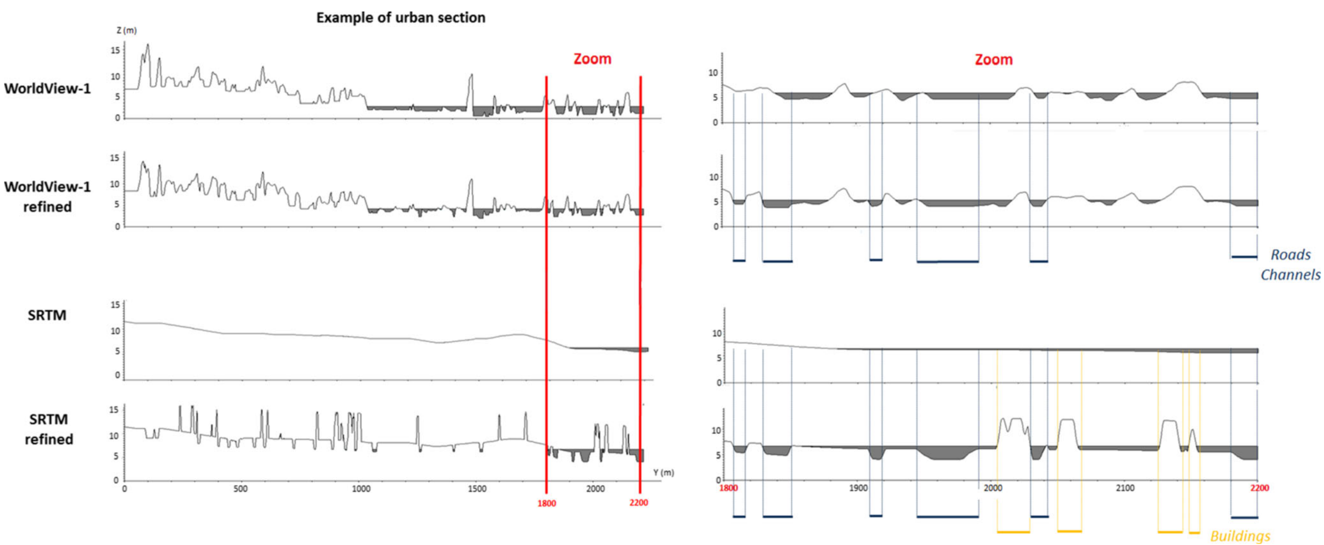

Fig. 6 Sample cross-section of the channel bed for the four scenarios created

available during hurricane Ike. Knowledge of rainfall amount, subsequent flood volume, and hydrograph shape are of paramount importance and exert a first-order control on flood dynamics and flooded areas. Downscaling of daily rainfall to an hourly resolution was deemed necessary, to reasonably depict the hydrological response of our catchment, displaying relatively small lag time (585 km^2, i.e. ca. 6 h lag time). To do so, we used a stochastic time random cascade approach, well assessed within the present literature (Bocchiola and Rosso, 2006; Groppelli et al., 2011a,b). No bias correction was possible, because no ground reference was available, so we had to assume that daily estimates from TRMM were accurate enough on average. Given the lack of hourly precipitation data necessary for calibration, the cascade parameters (i.e. rainfall intermittence β and cascade weights variance σ), providing intra-event duration of wet and dry periods and wet spells intensity, respectively, were reasonably taken according to similar studies in Italy and worldwide (e.g. Ravazzani et al., 2015) and are reported in Table 1.

The so downscaled precipitation was fed to a hydrological model to calculate the flood hydrograph for HEC-RAS 1D. Hydrological modelling of poorly gauged areas may be pursued using a suite of relatively simple models, mostly in the province of lumped flow routing and instantaneous unit hydrograph (IUH) theory (Bocchiola and Rosso, 2009; Grimaldi et al., 2013; Grimaldi and Petroselli, 2015). However, semi-distributed altitude belt or cell-based hydrological model can still be used if they require the least amount of information (Bocchiola et al., 2011). Here, we used a recently developed model, widely used with good results for hydrological modelling in many case study catchments worldwide (Confortola et al., 2013; Migliavacca et al., 2015, Soncini et al., 2015). This model mimics water-soil budget, by partitioning precipitation into liquid and solid (i.e. snow), and then liquid precipitation into soil moisture, evapotranspiration, and ground and overland (Hortonian) flow, and then provides semi-distributed flow routing of surface and subsurface runoff, so providing the flow hydrograph at the catchment outlet,

Table 1 Main properties of the La Quinte catchment. Adopted parameters for precipitation downscaling, and hydrological modelling. Explanation of the parameters and of their nature (lumped, spatially distributed, etc.) is reported. Estimation method is reported as well. For parameters derived from literature analysis, some references are provided for deeper insight

Par.	Exp.	Est.	Val.
Z_m [m a.s.l.]	Mean elevation	DEM	428
Z_{max} [m a.s.l.]	Maximum elevation	DEM	1460
Z_{min} [m a.s.l.]	Minimum, elevation	DEM	0
L_{mc} [km]	Main channel length	ARCGIS®, DEM	45
S_m [%]	Mean catchment slope	ARCGIS®, DEM	10
CN_m [.]	Mean curve number	ARCGIS®, land use	62
f_v [%]	Vegetated area	Land use	87
T_l [h]	Lag time overland	Bocchiola and Rosso (2009)	6.5
t_l [h]	Lag time ground	Groppelli et al. (2011b)	26
σ [.]	Variance of rainfall cascade	Bocchiola and Rosso (2006)	0.40
β [.]	Intermittence parameter rainfall cascade	Groppelli et al. (2011a)	0.01

at a proper (here, hourly) time scale. Flow routing from each single belt is carried out according to a geomorhologic-IUH method (Rosso, 1984). This model accounts for topographic structure of the catchment, while being little time consuming. Model setup only required use of (i) DEM (mostly available even at a low resolution), to evaluate altitude belts and expected catchment lag time (calculated as in Bocchiola and Rosso, 2009) and (ii) soil cover maps, for assessment of maximum soil storage S_{MAX}, to be used in the model within the soil moisture routing algorithm. The model uses a Hortonian approach to overland flow, occurring after soil saturation from below, i.e. when soil content reaches S_{MAX}. S_{MAX} value is estimated using the SCS-CN approach for reference, based upon land use classification from SPOT-5 (Fig. 7). However, it may be taken as a calibration parameter, to better simulate a measured hydrograph. Here, no hydrograph could be used for calibration, so S_{MAX} was fixed initially based upon soil use and held constant thenceforward. Evapotranspiration (ET) was neglected, because preliminary tests indicated that at the event scale, ET is considerably smaller than the other terms of the hydrological budget, i.e. infiltration and runoff. Also, given the tropical climate of the area, information of temperature trends with altitude, potentially usable to discriminate between liquid and solid precipitation was not necessary.

HEC-RAS 1D

HEC-RAS model used solves the full 1D St Venant equations for unsteady open channel flow, including floodplains flow, and it is often used as a benchmark for flood modelling (Horritt and Bates, 2002; Marzocchi et al., 2014). By dividing the flow area into a channel and a floodplain area, and assuming in each cross-section a horizontal water surface, with flow direction entirely normal, such that exchange of momentum between channel and floodplain may be neglected, and flow discharge is distributed according to conveyance into each zone, one has

$$\frac{\partial A}{\partial t} + \frac{\partial \phi Q}{\partial x_c} + \frac{\partial (1-\phi) Q}{\partial x_f} = 0 \quad (1)$$

and

$$\frac{\partial Q}{\partial t} + \frac{\partial}{\partial x_c}\left(\frac{\phi^2 Q^2}{A_c}\right) + \frac{\partial}{\partial x_f}\left(\frac{(1-\phi)^2 Q^2}{A_f}\right) + gA_c\left(\frac{\partial z}{\partial x_c}\right) + gA_f\left(\frac{\partial z}{\partial x_f} + S_f\right) = 0 \quad (2)$$

$$\phi = \frac{K_c}{K_c + K_f}, K = \frac{A^{5/3}}{nP^{2/3}} \quad (3)$$

$$S_c = \frac{\phi^2 Q^2 n_c^2}{R_c^{4/3} A_c^2}, S_f = \frac{(1-\phi)^2 Q^2 n_f^2}{R_f^{4/3} A_f^2} \quad (4)$$

where Q [m^3 s^{-1}] is the total flow, z [masl] is the elevation of the water surface, A_c and A_f [m^2] are the cross-sectional areas of the flow (in channel and floodplain), x_c and x_f are distances [m] along the channel and floodplain, P is the wetted perimeter, R [m] is the hydraulic radius (A/P), n is the Manning's roughness coefficient [m$^{-1/3}$ s] of floodplain n_f, and channel n_c, and S [.] is friction slope of floodplain S_f and channel S_c. The coefficient ϕ [.] indicates flow partitioning between floodplain ϕ_f and channel $\phi_c = 1 - \phi_f$, according to the respective conveyances, K_c and K_f. This set of equation is numerically approximated and solved by way of an implicit finite difference scheme (USACE, 2010). Nowadays, two-dimensional (2D) inundation models are wide spread for flood hazard

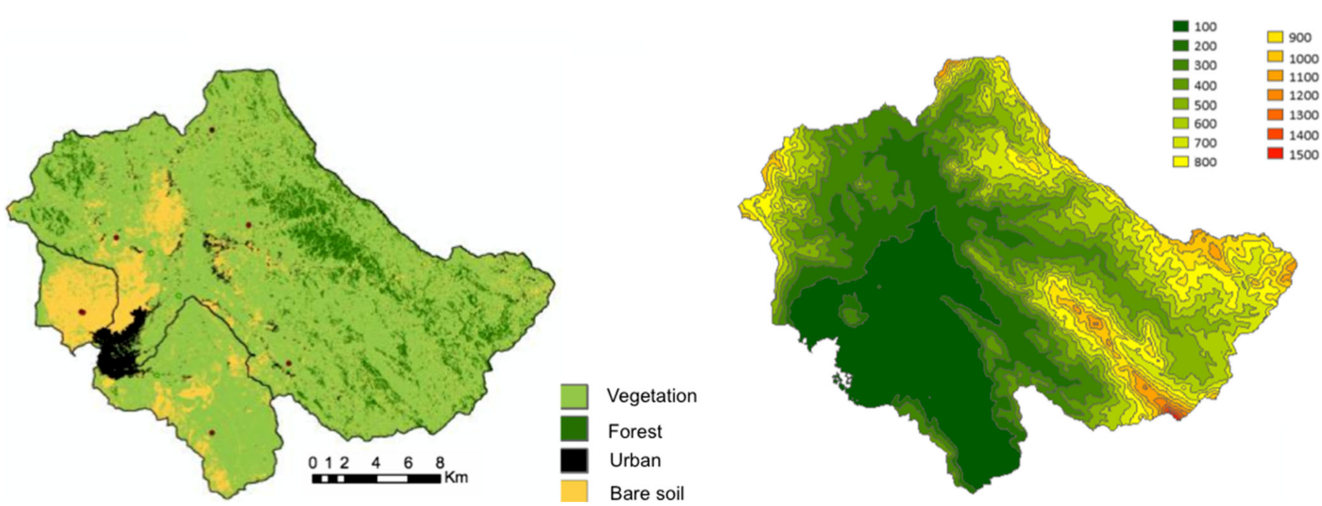

Fig. 7 La Quinte river catchment. Distributed land use map (*left*), and DEM (altitude in meters above sea level (*masl*), *right*)

mapping worldwide (Neal et al., 2012). Bi-dimensional models may provide more refined description of flow characteristics within the flood domain, especially velocity, strongly driven by topography. However, in principle, 2D models require longer simulation times and a reasonable knowledge of hydraulic roughness and of its spatial distribution. Usually, optimized roughness coefficient may be obtained by way of model tuning against observed flood hydrograph and, in channel flow velocity, observed flow depth (and velocity) within the floodplain (e.g. Horritt and Bates, 2002) or other proxies. Also, while spatially variable values of roughness should be used in floodplains; more often than not, one single value is used, normally tuned against flooding data (e.g. Horritt, 2006). HEC-RAS model requires a minimum amount of input data, and it is computationally efficient if compared to the more complex 2D model (Horritt et al., 2007). Furthermore, in some cases HEC-RAS model may be appropriate also in predicting flood extent (Brandimarte et al., 2008). Given the total lack of hydrometric data to validate both in stream and floodplain roughness and of direct observation of flow depth and velocity anywhere in the study area, use of a 2D model here seems far-fetched. Notice also that, here, strong uncertainty dwells into estimated flood volume, available only through TRMM rainfall estimates, which is the most important driver of flooded areas extent (e.g. Horritt and Bates, 2002). HEC-RAS model solves continuity (mass conservation) and momentum conservation equations above within the domain of the flood, including the whole flooded area by construction. Accordingly, flood volume is accounted for and inundation volume is already consistent. In this sense, use of a 2D model under lack of data as reported would likely add more uncertainty and provide little improvement.

Model setup

HEC-RAS has been set up to cover a 15-km^2 reach around the urban area of Gonaives, Haiti (Fig. 1). Channel geometry was set up using a series of 48 cross-sections, at 200 m steps, along the stream centerline. These sections were extended on both sides of the channel using information from SRTM and WorldView-1, to provide floodplain topography. In terms of elevation models, we used four different DEM scenarios for each simulation, namely the original WorldView-1 and SRTM DEMs and the corresponding refined DEMs. These topographic data are interpolated by HEC-GeoRAS upon each of the 48 cross-sections. Setup of HEC-RAS model requires a number of items.

First, Manning's roughness coefficients are needed. Geometric information was imported from GIS software to each of 500 points taken along the 48 cross-sections. The simulations were carried out using two different bed roughness coefficients for channel and floodplain, as often done within the present literature to assess model performance in predicting inundation (Horritt et al., 2002). We then carried out a sensitivity analysis, by varying channel and floodplain values in the plausible range of $0.011 < n < 0.15\ \mathrm{m}^{-1/3}\ \mathrm{s}$.

Then, a flood hydrograph is required, either considering steady (constant flow in time) or unsteady (variable flow) flow. Use of unsteady flow hydrographs for simulation of flooded areas may be cumbersome and time consuming. Steady flow simulation may in turn provide a rapider tool for assessment of potentially inundated areas, when time is limited. We simulated both steady and unsteady flow, to test the potential of both for flooding area simulation in our case study. Steady flow analysis has been carried out here by taking a constant flow rate given by the highest (hourly peak) discharge that we obtained (1114 $\mathrm{m^3 s^{-1}}$). The boundary conditions entered are imposed by taking the normal depths as per slope of the channel bottom, namely 0.0043 at the upstream and downstream ends, calculated via ArcGIS. Unsteady flow simulation requires varying boundary conditions. We used the modeled flow hydrograph as an upstream condition and normal depth as a downstream condition. We did not use lateral contributions given the limited increase of contributing area in town. The simulation period we used is of 10 days around hurricane Ike episode, with fixed start time on 30 August at 0000 hours and end on 9 September at 2300 hours.

HEC-GeoRAS, an ArcGIS extension, was employed to generate geospatial data from HEC-RAS output information. We obtained overall 80 flood extent map simulations that were subsequently validated based upon accuracy criteria.

Model validation

The degree of accuracy of mapped flooded areas may be estimated by the closeness between our numerical solution, i.e. HEC-RAS simulation, and the "ground truth", i.e. the flood map generated from SPOT-4 image, being aware that even the latter may entail noise and inaccuracies. As often done in the literature, the agreement between the model simulated and the satellite observed maps was evaluated using a Jaccard's similarity index (e.g. Wilson and Atkinson, 2007), given as

$$S_j = \frac{A_{\mathrm{obs}} \cap A_{\mathrm{sim}}}{A_{\mathrm{obs}} \cup A_{\mathrm{sim}}} \tag{5}$$

where A_{obs} is the observed inundated area (flood map generated from SPOT-4 image) and A_{sim} (HEC-RAS simulations) is the simulated inundated area. The symbols ∩ and ∪ denote intersection (i.e. concordance of observed and simulated inundated areas) and union (i.e. sum of observed and simulated inundated areas), respectively. S_j varies between 0 and 1, with 1 for perfect agreement. Jaccard's index as defined in Eq. (5) is not able to discriminate the difference between overestimation and underestimation of the flooded areas. Even if observed flooded areas (i.e. in the image, A_{obs}) are well depicted by the model ($A_{obs} \cap A_{sim}$) excessive flooding from the model (i.e. too large inundated area A_{sim}) is paid with a decrease of S_j (because $A_{obs} \cup A_{sim}$ increases). We thus introduced another index S_i, which we called intersection similarity index, namely

$$S_i = \frac{A_{obs} \cap A_{sim}}{A_{obs}} \quad (6)$$

which gives information concerning the actual capacity of the model to depict flooded areas according to the satellite image, regardless of the extent of the modelled flooded areas. We used S_j and S_i, to select the "optimal" (largest S_j, S_i) scenarios for flood simulation against Manning's coefficients with a sensitivity analysis (Horritt and Bates, 2002). Given the different pixel size between simulation results and observed flooded area, we used for validation a series of random points within the simulation domain. We changed the number of points, from 1500 to 750,000 random points or from one point every 10,000 m^2 to one point every 400 m^2 (pixel size of SPOT-4 image). Although use of more points progressively increases the stability of the adaptation indexes (S_j and S_i), use of 1500 points still provides accurate parameters' (Manning's coefficients) identification. Then, using the so obtained values of Manning's coefficients, we carried out a sensitivity analysis of S_j and S_i against the threshold of water depth for proper identification of flooded areas. In fact, labelling of flooded areas for low water depth may potentially provide overestimation of the flooded areas.

Results

Flood hydrograph

In Fig. 8, we report the hourly (and corresponding average daily) downscaled precipitation and subsequently calculated hydrograph. The highest (peak) discharge we obtained is 1114 m3 s^{-1} at September 1 15:00, and the estimated flood volume (August 3–September 9) was of 9.18×10^7 m^3. We preliminarily tested different realizations of the precipitation pattern (conserving average rainfall from TRMM) according to use of the random cascade, and no sensible differences were seen either in the flood hydrograph or in the flooding volume, so no noticeable change occurs in the flooding area. Initial soil moisture condition may affect the results. Given that no large rainfall events occurred in the few days before the event, the assumption of relatively dry soil at the onset of the Hurricane was made. Flood event 1 in Fig. 8 (occurring on September 1) started at 10 a.m. ca., after the onset of intense rainfall starting at midnight of September 1, with 9 mm h^{-1} on average daily. So overland flow occurred with ca. 99 mm of rainfall in 11 h. Event 2 instead started at midnight of September 6, with 2.5 mm h^{-1} rainfall on average daily. However, at 8:00 a.m. of the same day, overland flow occurred and flow discharge increased rapidly, after only a few millimetres of rain (ca. 22.5 mm). Clearly, albeit the two flood events were separated by few days (and the two peaks were 5 days apart from each other), still event 2 occurred because event 1 had largely saturated the soil, providing the conditions for further flooding. Given also that our flood map from SPOT-4 dated September 9, 2008, as reported, we deemed necessary to consider both flood events in our exercise.

Flooding maps

We tested flood mapping performance using (i) steady or unsteady hydrograph, (ii) differently refined elevation models, and (iii) different Manning roughness coefficients (i.e. sensitivity analysis). In Fig. 9, a graphic summary of Jaccard's similarity index S_j and of intersection index S_i for our simulations is given, and the results therein can be resumed as follows. In steady flow regime, the validation index S_j ranges between 63 and71 % using WorldView DEM (S_i, 79–95 %), 63 and 72 % using WorldView DEM refined (S_i, 77–95 %), 49 and 59 % using SRTM (S_i, 58–80 %), and 56 and 67 % using SRTM refined (S_i, 67–88 %). The best (highest S_j) simulation was attained using a Manning value of 0.011 $m^{-1/3}$ s in channel and of 0.15 $m^{-1/3}$ s in floodplains, for all DEMs, except for SRTM, the latter has quite low S_j. Generally speaking, S_i follows a similar pattern as S_j, albeit higher absolute values, likely indicating reasonable overlapping with actually (i.e. from the satellite) flooded areas, at the cost of too large flooded areas from the model.

As far as unsteady simulation is concerned, the performance is generally more stable (i.e. the model seems less sensitive to Manning's coefficient), except for SRTM DEM, which again delivers comparatively low accuracy. S_j ranged within 69–73 % ($S_i > 95$ %) using WorldView DEM, 69–72 % using WorldView DEM refined ($S_i > 95$ %), 51–61 % using SRTM (S_i, 66–84 %), and 66–70 % using SRTM refined (S_i ca. 94 %). In Figs. 10 and 11, we report the flooded areas by the model, using the best fit (according to S_j) Manning's values in Fig. 9, for steady and unsteady simulation, respectively, to aid visual assessment of the model's performance.

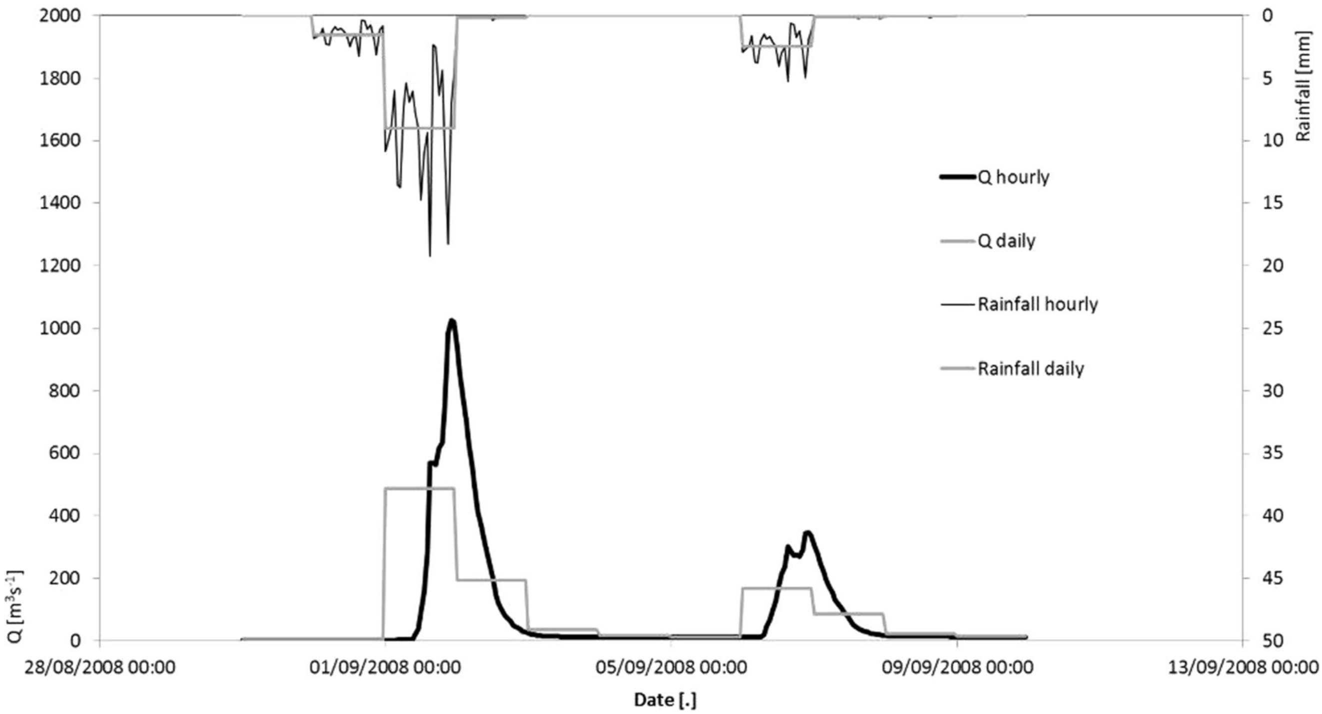

Fig. 8 Daily observed and hourly downscaled precipitation and simulated hourly discharges

In Fig. 12, we report the sensitivity of S_j and S_i (side Table) to threshold water depth for the two cases of Worldview-1, WV original and SRTM refined, steady and unsteady, starting from a 1-cm to 1-m depth flow area. We used therein the best fit simulation (S_j) for Manning's coefficient. We selected these two DEMs given that WV original DEM would not profit from noticeable improvement in flood extent simulation when refined (Fig. 9), whereas SRTM DEM would attain considerable improvement after refining. Apparently in all cases, and for both S_j and S_i, a best threshold is attained for the range 0–0.1 m, with substantially constant values (and a slight peak for SRTM refined for unsteady flow) and with loss of accuracy

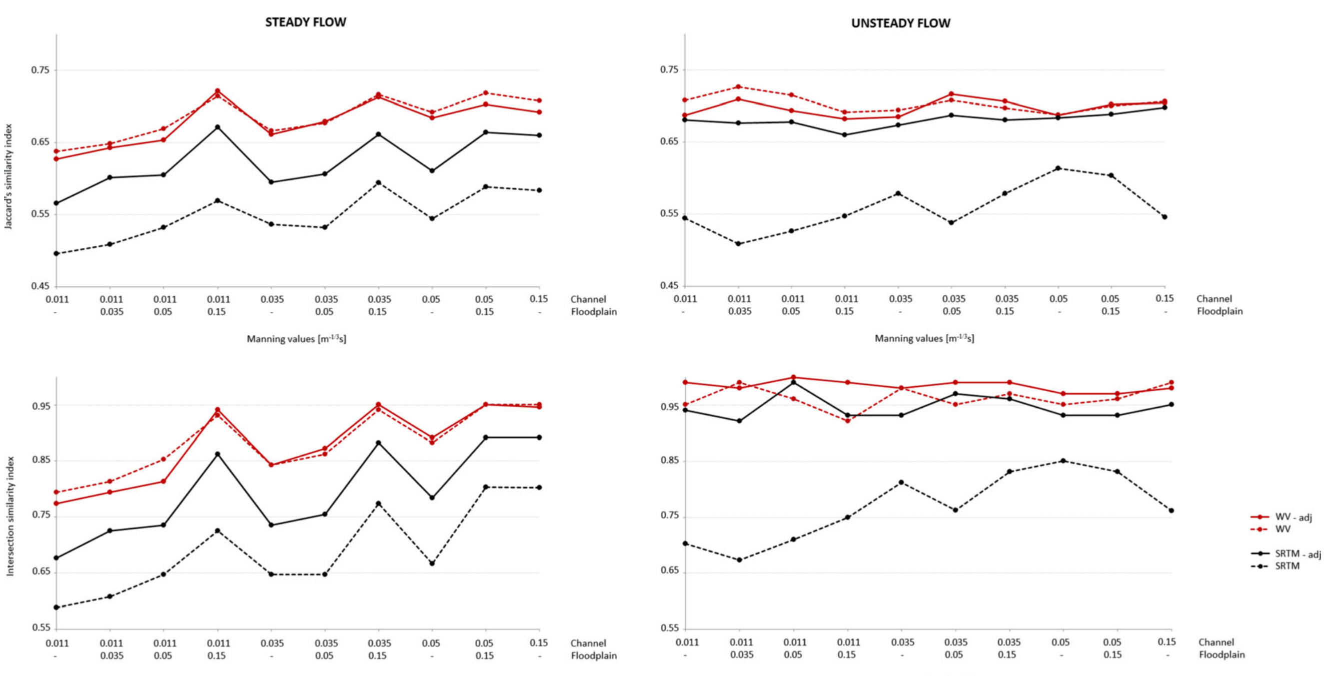

Fig. 9 Summary of Jaccard's similarity index. Steady and unsteady flow of the four DEM scenarios

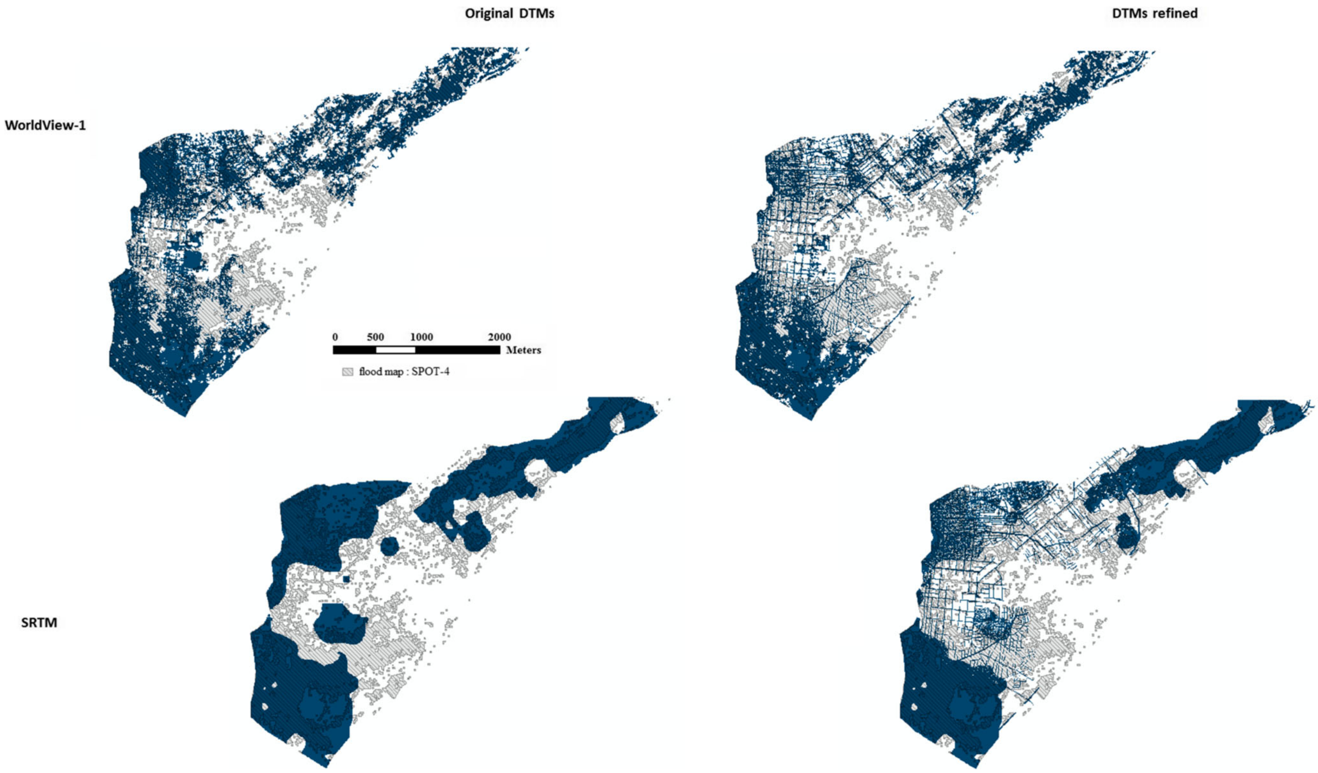

Fig. 10 Steady flow regime. Best fit (S_j) water simulation extent using Manning's values in Fig. 9 for each DEM

for increasing depths until 1 m. Accordingly, agreement between model's simulation and satellite image depends upon the least significant water depth assumed in the simulation, but within a relatively broad range.

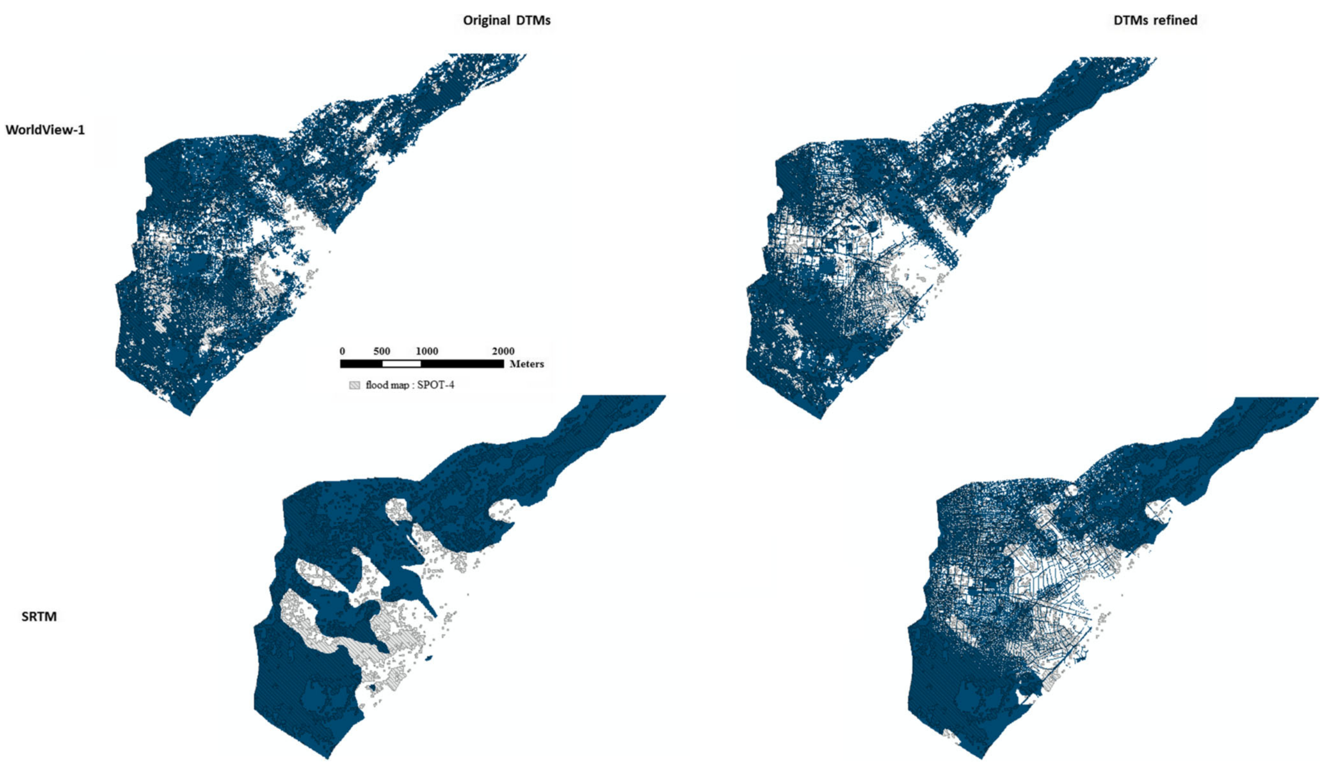

Fig. 11 Unsteady flow regime. Best fit (S_j) water simulation extent using Manning's values in Fig. 9 for each DEM

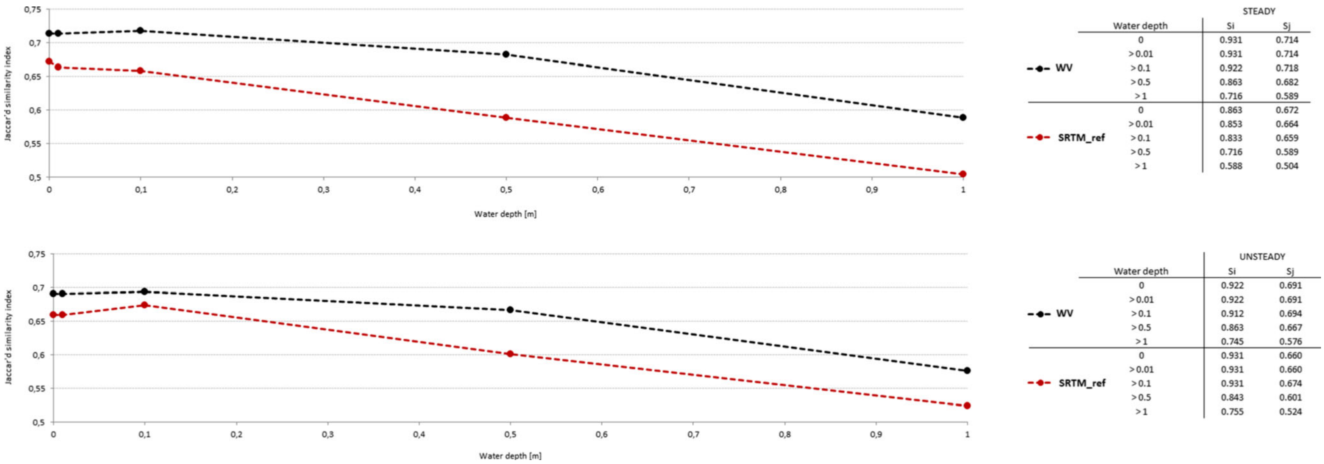

	Water depth	STEADY Si	STEADY Sj
WV	0	0.931	0.714
	>0.01	0.931	0.714
	>0.1	0.922	0.718
	>0.5	0.863	0.682
	>1	0.716	0.589
SRTM_ref	0	0.863	0.672
	>0.01	0.853	0.664
	>0.1	0.833	0.659
	>0.5	0.716	0.589
	>1	0.588	0.504

	Water depth	UNSTEADY Si	UNSTEADY Sj
WV	0	0.922	0.691
	>0.01	0.922	0.691
	>0.1	0.912	0.694
	>0.5	0.863	0.667
	>1	0.745	0.576
SRTM_ref	0	0.931	0.660
	>0.01	0.931	0.660
	>0.1	0.931	0.674
	>0.5	0.843	0.601
	>1	0.755	0.524

Fig. 12 Sensitivity of S_j and S_i to threshold of water depth for the two cases of WV original and SRTM refined, steady and unsteady

Discussion

Our findings here provide room for some discussion. We simulated inundated flood areas for the case of Gonaives, Haiti, where a least amount of remotely gathered data is available, and orthodox flood mapping exercise according to state-of-the-art techniques is borderline feasible. We set up a simple hydrological model using only DEM and land use information and fed it with TRMM data, and we carried out flow routing and flood simulation by way of a 1D model, plus high-resolution urban mapping from different remote sensing devices, including the open web source OpenStreetMap; the latter was used to describe precisely small-scale topography, an utmost importance for flood depiction. Validation of our model could only be carried by way of remotely measured flooded areas. In Figs. 10 and 11, we reported the extent of the best simulations from WordView-1 and SRTM, original and refined, steady and unsteady, overlapping to the SPOT-4 image (after flood). The simulations seem to depict acceptably the satellite-estimated flood extent. Visually, unsteady flows seem to provide a larger share of correctly identified flooded areas $A_{obs} \cap A_{sim}$, as well as larger inundation extent. Refinement of WV DEM using OpenStreetMap does not carry visible improvement of mapping performance, while SRTM improves considerably after refinement, displaying how DEM manipulation based upon open sources may help to reach improved topographic detail for flood mapping. Both adaptation indexes S_j and S_i display some dependence upon Manning's coefficients within channel and floodplain, but more visibly for steady flow. Index S_j is normally higher (and less variable) for the unsteady simulation, than for the steady one, implying that flood mapping according to variable flow captures the inundation phenomena better than use of permanent flow.

Unsteady flow simulation is especially outperforming steady routing according to S_i index (Fig. 7), which is always higher in the unsteady plot, and constantly close to 95 % therein, except for SRTM unrefined. The decrease in S_j vs S_i, seen especially for unsteady flow, is clearly due to larger inundation extent in this case (i.e. to increase of $A_{obs} \cup A_{sim}$ in Eq. 5). Accordingly, one notices that use of different adaptation indexes provides different perceptions of the model accuracy.

Specifically, intersection index S_i displays the capability of the model to fit the satellite-estimated flooded areas, regardless of potential model's overestimation. Jaccard's index S_j on the other hand penalizes overestimation of flooded areas, clearly avoiding the chance of capturing flooded area by simulating flooding everywhere. The choice of privileging either of the two approaches is possibly subjective. However, one can put forward the idea that in case one is interested into predicting the areas that are most prone to flooding for land use planning and early warning purposes, it may be more important to accurately depict flooded areas at the cost of overestimating the flooded extent, than vice-versa. In this sense, large values of S_i, possibly coming with acceptable values of S_j (i.e. with reasonable overestimation) may be an asset of the procedure. Here, large values of S_i (nearby 95 % or so) are reached, especially when using unsteady flood routing (except for the very coarse SRTM DEM), which may imply that the flood mapping chain used here does provide acceptable coverage of potentially floodable areas. For instance, when considering unsteady flow, taking an average value of $S_i = 0.95$ (except for SRTM) and a corresponding average value of $S_j = 0.70$, one has that 95 % of flooded areas captured, 5 % are not, and the model provides flooding overestimation of 30 % in absolute area, rising to 35 % when considering misplacement. Considering steady flow, and similarly for WV original and refined, one has in the best case $S_i = 0.95$, $S_j = 0.72$, i.e. overestimation of 26 % in absolute area and 31 % when considering misplacement, and in the worst case, $S_i = 0.77$ (i.e. 23 % flooded area uncovered) and $S_j = 0.61$, i.e. overestimation of only 3 % in absolute area, but 26 % with misplacement. For SRTM DEM refined, one has a best case of

S_i = 0.88 and S_j = 0.67, with overestimation of 20 %, and misplacement of 32 %, and a worst case of S_i = 0.67 and S_j = 0.56, with underestimation of −13 % in absolute value but 33 % with misplacement.

Sensitivity to Manning's coefficients displayed in Fig. 9 indicates some variability of the performance when using the steady mode, while little changes occur against Manning's coefficients when unsteady mode is used (except for SRTM mode, however, with worse performance). This seems to suggest that under the unsteady mode, the flood mapping area is little sensitive to Manning's coefficients setting and choice of an optimal set of roughness coefficients is hardly feasible. Given that Manning's coefficient basically influences flow velocity and consequently inundation timing, one may hypothesize that when unsteady flow is considered, flood modelling and inundated areas are possibly governed by flood volume, somewhat independently of flow velocity. Concerning steady flow, where a constant discharge is used and flood volume is substantially not influent, spatial occupation is slightly more dependent upon roughness.

Given that no flow velocity data are available, such hypothesis can be hardly verified. Verification of in-channel roughness could be potentially carried out using, e.g. an observed in-channel travel time of the flood wave (Horrit and Bates, 2002), whenever available, and ideally floodplain roughness may be tested against flood images taken at different times during the flood event; however it is not available here. Assessment of flooded areas pending largely uncertain hydraulic parameters as here may be carried out by more complex approaches, e.g. by way of Monte Carlo simulation of roughness parameter under a generalized likelihood uncertainty estimation (GLUE) approach, to define area (pixel)-based flooding probability (Aronica et al., 2002). Such methods provide spatially distributed probability of inundation and can be used for prognostic purposes, provided a priori information is available about spatially distributed model's performance (i.e. S_j here). However, such approach seems beyond our explorative framework here, and given the lack of data for the area, we may not be able to check its potential for flood prediction.

The sensitivity analysis against the threshold water depth for inundation by the model (Fig. 12) seemingly to indicate taking water depth above 10 cm may provide an accurate enough depiction of flooding, without large loss of information (and even with slight gain in accuracy). Such threshold seems consistent with the present literature and may be used to avoid flood overestimation linked to topographic noise (Aronica et al., 2002).

Further potential uncertainty may dwell within the hydrological model is the choice of S_MAX, controlling overland flow volume. S_MAX is distributed in space and evaluated here according to observed soil properties, using widely adopted methodologies based upon guided classification, as supported within the present literature (based on SCS-CN, 1986). Lag time is calculated against physical attributes, using a calibrated formula from literature, so physically based and a priori estimated. Given that here, flood discharges are not available, there is no chance of calibration of these parameters using an a posteriori approach. Flood hydrograph shape is little sensitive as reported to downscaling, and so is the flood volume, so this facet would not impact largely on our results. However, flow measurements in the area are an utmost need.

The reference accuracy obtained when benchmarking inundated areas against remote sensing data need be known, given that even a perfectly performing inundation model will never be able to reach a higher nominal accuracy than the reference (image) one when compared against the sole image (Horritt and Bates, 2002). Here, no estimate of such reference accuracy is possible in our understanding given the lack of ground data. Therefore, good matching of the model to the observed flooded areas may be generally taken as indicative of a good performance, but a stringent comparison is not feasible hitherto in this sense.

The best performing DEM we found here was the WV, which performed equally well in the original and refined mode. The SRTM model instead improved largely when refined. However, original SRTM DEM is very coarse (90 m, Fig. 4), and clearly refining provides largely increased depiction of topography. Contrarily, WV DEM is in its original version is already fine enough (0.5 m, Fig. 4) that it can afford accurate flood simulation, and further refining seems not to increase its performance. Some criticalities may be highlighted in the DEM refinement procedure using our approach. The accuracy of the refined DEM depends upon the accuracy of the OpenStreetMap items, which is therefore crucial. In case of a rapid increase in population density (building construction), a DEM could become quickly up to date. An example of this is given by differences in building textures in WorldView-1 and SRTM refined, in Fig. 4. WorldView-1, dating 2010, has more buildings than SPOT-5, dating 2007, and used to detect and extrude building into SRTM refined.

Conclusions

The mapping for flood inundation depth and extent using hydraulic modelling is an essential component of flood risk management practice worldwide (Neal et al., 2013). Our study focusing on Gonaives, Haiti, where a tremendous lack of ground data occurs, provides acceptable results in depicting flooded areas therein for hurricane Ike in 2008, with flooded area matching up to 95 %. Keeping in mind the aims of aiding flood risk assessment and land use planning, and of forecasting of floods during large storm events, our study displays the considerable potential of information from remote sensing imagery and from open street databases to support hydrological and hydraulic modelling towards such ends. We displayed that initially coarse digital elevation models such as SRTM may provide improved depiction of flooded areas after a refinement procedure based upon the data from open street databases. The simulated inundation areas likely suffered from uncertainty dwelling into flood hydrograph simulation, introduced by (i) noise within TRMM rainfall estimates, (ii) stochastic noise within hourly downscaling, albeit here little disturbing as reported, and (iii) lack of tuning of the hydrological model. In the future, if rainfall and discharge data will continue lacking, some way to validate both will be needed. According to such findings, our research will look for further refinements by validating the simulation results with better spatial resolution (after flood) images whenever they would arise, testing our approach on other extreme flood events, using other free or institutional GIS database to better refine DEMs and using DEMs with close as possible acquisition date. Further on, we will need to compare 2D hydraulic modelling results against 1D. Whenever the procedure proposed here could be automated, delineation of (either real or potential, e.g. under an either observed or designed storm scenario) flooded areas may guide first aid intervention during extreme flood events, evaluate water ponding extent and duration, and provide extra information to lead simulation of, and intervention on, spreading of waterborne diseases, within poorly gauged areas, as in our case study in Gonaives, Haiti. Ideally, the approach proposed here may aid in depiction of flooded areas for extreme flood events in other regions worldwide, as it may be implemented using datasets with world coverage and simple hydrological and hydraulic tools.

Acknowledgments The presented work took place during Eng. Bozza's internship and was carried out in cooperation between SERTIT institute (University of Strasbourg) and DICA Dept., Hydrology Division (Politecnico di Milano). The authors wish to acknowledge KAL-Haiti project and International Charter Space and Major Disaster. The KAL-Haiti project is funded by the French Agence Nationale de la Recherche (ANR) under grant number 2010 HAIT 008 01. Contributions of data providers to the database, whose list is available on the Kal-Haiti website, are acknowledged by the KAL-Haiti project team. Dr. Gabriele Confortola acknowledges contribution from "I-CARE" project, funded under the 5 % scheme from Politecnico di Milano, year 2009. Two anonymous reviewers are kindly acknowledged for their useful comments.

References

Aronica G, Bates PD, Horritt MS (2002) Assessing the uncertainty in distributed model predictions, using observed binary pattern information within GLUE. Hydrol Process 16:2001–2016

Bates PD, Horritt MS, Smith CN, Mason DC (1997) Integrating remote sensing observations of flood hydrology and hydraulic modelling. Hydrol Process 11:1777–1795

Bates PD, Marks KJ, Horritt MS (2003) Optimal use of high resolution topographic data in flood inundation models. Hydrol Process 17: 5237–5557

Bates PD (2004) Remote sensing and flood inundation modelling. Hydrol Process 18:2593–2597

Bates PD (2012) Integrating remote sensing data with flood inundation models: how far have we got? Hydrol Process 26:2515–2521

Bocchiola D, Rosso R (2006) The use of scale recursive estimation for short term quantitative precipitation forecast, physics and chemistry of the earth 2006: 31, 18:1228–1239.

Bocchiola D, Rosso R (2009) Use of a derived distribution approach for extreme floods design: a case study in Italy. Adv Water Resour 32(8):1284–1296

Bocchiola D, Diolaiuti G, Soncini A, Mihalcea C, D'Agata C, Mayer C, Lambrecht A, Rosso R, Smiraglia C (2011) Prediction of future hydrological regimes in poorly gauged high altitude basins: the case study of the upper Indus, Pakistan. Hydrol Earth Syst Sci 15:2059–2075

Brandimarte L, Brath A, Castellarin A, Di Baldassarre G (2008) Isla Hispaniola: a trans-boundary flood risk mitigation plan. Phys Chem Earth 34:209–218

Confortola G, Soncini A, Bocchiola D (2013) Climate change will affect water resources in the Alps: a case study in Italy. J Alpine Res *RGA/JAR* 101(3):1–15

Di Baldassarre G, Schumann G, Bates PD (2009) A technique for the calibration of hydraulic models using uncertain satellite observations of flood extent. J Hydrol 367:276–282

FRANCE24, 2013: http://www.france24.com/fr/.

French JR (2003) Airborne LiDAR in support of geomorphologicaland hydraulic modelling. Earth Surf Process Landf 28(3):321–335

Gomes-Pereira LM, Wicherson RJ (1999) Suitability of laser data for deriving geographical data: a case study in the context of management of fluvial zones. Photogramm Remote Sens 54:105–114

Grimaldi S, Petroselli A, Romano N (2013) Green-Ampt Curve-Number mixed procedure as an empirical tool for rainfall-runoff modelling in small and ungauged basins. Hydrological Processes, Vol. 27, p. 1253–1264, ISSN: 1099–1085, doi:10.1002/hyp.9303.

Grimaldi S, Petroselli A (2015) Do we still need the rational formula? An alternative empirical procedure for peak discharge estimation in small and ungauged basins. Hydrol Sci J 60(1):67–77

Groppelli B, Bocchiola D, Rosso R (2011a) Spatial downscaling of precipitation from GCMs for climate change projections using random cascades: a case study in Italy. Water Resour Res 47:W03519

Groppelli B, Soncini A, Bocchiola D, Rosso R (2011b) Evaluation of future hydrological cycle under climate change scenarios in a mesoscale Alpine watershed of Italy. Nat Hazard Earth Syst Sci 11:1769–1785

Horritt MS (2000) Calibration and validation of a 2-dimensional finite element flood flow model using satellite radar imagery. Water Resour Res 2000 36(11):3279–3291

Horritt MS, Mason DC, Luckman AJ (2001) Flood boundary delineation from synthetic aperture radar imagery using a statistical active contour model. Int J Remote Sens 22(13):2489–2507

Horritt MS, Bates PD (2002) Evaluation of 1D and 2D numerical models for predicting river flood inundation. J Hydrol 268:87–99

Horritt MS (2006) A methodology for the validation of uncertain flood inundation models. J Hydrol 326(1–4):153–165

Horritt MS, Di Baldassere G, Bates PD, Brath A (2007) Comparing the performance of 2-D finite element and finite volume models of floodplain inundation using airborne SAR imagery. Hydrol Process 21(20):2745–2759

Hunter NM, Bates PD, Horritt MS, De Roo APJ, Werner MGF (2005) Utility of different data types for calibrating flood inundation models within a GLUE framework. Hydrol Earth Syst Sci 9(4):412–430

Marks K, Bates PD (2000) Integration of high resolution topographic data with floodplain flow models. Hydrol Process 14:2109–2122

Marzocchi R, Federici B, Cannata M, Cosso T, Syriou A (2014) Comparison of one-dimensional and two-dimensional GRASS-GIS models for flood mapping. Appl Geomatics 6(4):245–254

Mason DC, Bates PD, Dall'Amico JT (2009) Calibration of uncertain flood inundation models using remotely sensed water levels. J Hydrol 368:224–236
Migliavacca G, Confortola A, Soncini A, Diolaiuti A, Smiraglia C, Barcaza G, Bocchiola D (2015) Hydrology and potential climate changes in the Rio Maipo (Chile). Geografia Fisica e Dinamica Quaternaria GFDQ 38(2):155–168
Neal J, Keef C, Bates P, Beven K, Leedal D (2013) Probabilistic flood risk mapping including spatial dependence. Hydrol Process 27: 1349–1363
Neal J, Villanueva I, Wright N, Willis T, Fewtrell T, Bates P (2012) How much physical complexity is needed to model flood inundation? Hydrol Process 26:2264–2282
NOAA (National Oceanic Atmospheric Administration) (2012): <http://www.noaa.gov/about-noaa.html.
Ravazzani G, Bocchiola D, Groppelli B, Soncini A, Rulli MC, Colombo F, Mancini M, Rosso R (2015) Continuous stream flow simulation for index flood estimation in an Alpine basin of Northern Italy. Hydrol Sci J 60(6):1013–1025
Rinaldo A, Bertuzzo E, Mari L, Righetto L, Blokesch M, Gatto M, Casagrandi R, Murray M, Vesenbeckh SM, Rodriguez-Iturbe I (2012) Reassessment of the 2010-2011 Haiti cholera outbreak and rainfall-driven multiseason projections. PNAS 109(17):6602–6607
Rosso R (1984) Nash model relation to Horton order ratios. Wat Resour Res 20(7):914–920
Sanders B (2007) Evaluation of on-line DEMs for flood inundation modelling. Adv Water Resour 30:1831–1843
Satimagingcorp, Satellite Imaging Corporation, Worldview (2012): http://www.satimagingcorp.org/
Schumann G. Bates PD, Horritt M, Matgen P, Pappenberger F (2009). Progress in integration of remote sensing derived flood extent and stage data and hydraulic models. Reviews of Geophysics 47, no. RG4001.
Smith LC (1997) Satellite remote sensing of river inundation area, stage and discharge: a review. Hydrol Process 11(10):1427–1439
Soil Conservation Service (1986). Urban hydrology for small watersheds, U.S. Department of Agriculture, Washington D.C., 1975, Updated, 1986.
Soncini A, Bocchiola D, Confortola G, Bianchi A, Rosso R, Mayer C, Lambrecht A, Palazzi E, Smiraglia C, Diolaiuti G (2015) Future hydrological regimes in the upper Indus basin: a case study from a high altitude glacierized catchment. J Hydrometeorol 16(1):306–326
SRTM (NASA) (2012): http://www2.jpl.nasa.gov/srtm.
Stephens EM, Bates PD, Freer JE, Mason DC (2012) The impact of uncertainty in satellite data on the assessment of flood inundation models. J Hydrol 414–415:162–173
USACE, US Army Corps of Engineers (2010) HEC-RAS River analysis system, Hydraulic Reference Manual, Version 4.1.
Wilson MD, Atkinson PM (2007) The use of remotely sensed land cover to derive floodplain friction coefficients for flood inundation modelling. Hydrol Process 21(26):3576–3586
Yamazaki D, Calum A, Bates PD, Kanae S, Douglas E, Taikan O (2012) Adjustment of a spaceborne DEM for use in floodplain hydrodynamic modelling. J Hydrol 81(9):436–437
Yesou H, Clandillon S, Allenbach B, Inglada J, Favard JC, Bestault C, de Fraipont P (2003). A constellation of advantages with SPOT SWIR and VHR SPOT 5 data for flood extent mapping during the September 2002 Gard event (France). IGARSS 2003: IEEE International geoscience and remote sensing symposium, vol I–VII, Proceedings: Learning From Earth's Shapes And Sizes, 567–569.